Acta Cryst C STRUCTURAL CHEMISTRY

ISSN 2053-2296

Crystal structure, thermal properties and detonation characterization of bis(5-amino-1,2,4-triazol-4-ium-3-yl)methane dinitrate

Hongya Li,[a] Biao Yan,[a]* Haixia Ma,[b] Xiangrong Ma,[a] Zhiyong Sun[c] and Yajun Ma[a]

[a]School of Chemistry and Chemical Engineering, Yulin University, Yulin, Shaanxi 719000, People's Republic of China, [b]School of Chemical Engineering, Northwest University, Xi'an, Shaanxi 710069, People's Republic of China, and [c]School of Energy Engineering, Yulin University, Yulin, Shaanxi 719000, People's Republic of China. *Correspondence e-mail: yanbiaoly@foxmail.com

Received 1 August 2020
Accepted 12 September 2020

Edited by A. Sarjeant, Bristol-Myers Squibb, USA

Keywords: 1,2,4-triazole; BATZM dinitrate; crystal structure; thermodynamics; quantum chemistry; detonation characterization.

CCDC reference: 1060498

Supporting information: this article has supporting information at journals.iucr.org/c

Bis(5-amino-1,2,4-triazol-4-ium-3-yl)methane dinitrate, BATZM·$(NO_3)_2$ or $C_5H_{10}N_8^{2+}\cdot 2NO_3^-$, was synthesized and its crystal structure determined by single-crystal X-ray diffraction. It crystallizes in the space group *Pbcn* (orthorhombic) with $Z = 4$. BATZM·$(NO_3)_2$ is a V-shaped molecule where hydrogen bonds form a two-dimensional corrugated sheet with reasonable chemical geometry and no disorder. The specific molar heat capacity ($C_{p,m}$) of BATZM·$(NO_3)_2$ was determined using the continuous C_p mode of a microcalorimeter and theoretical calculations, and the $C_{p,m}$ value is 366.14 J K^{-1} mol^{-1} at 298.15 K. The relative deviations between the theoretical and experimental values of $C_{p,m}$, $H_T - H_{298.15K}$ and $S_T - S_{298.15K}$ of BATZM·$(NO_3)_2$ are almost equivalent at each temperature. The detonation velocity (D) and detonation pressure (P) were estimated using the nitrogen equivalent equation according to the experimental density; BATZM·$(NO_3)_2$ has a higher detonation velocity (7927.47 ± 3.63 m s^{-1}) and detonation pressure (27.50 ± 0.03 GPa) than 2,4,6-trinitrotoluene (TNT). The above results for BATZM·$(NO_3)_2$ are compared with those of bis(5-amino-1,2,4-triazol-3-yl)methane (BATZM) and bis(5-amino-1,2,4-triazol-4-ium-3-yl)methane dihydrochloride (BATZM·Cl_2), and the effect of nitrate formation is discussed.

1. Introduction

Nitric acid is a strong acid with strong oxidizing properties, and many nitrates can be used in pyrotechnics, explosives or propellants. For example, triaminoguanidine nitrate is used in gunpowder; urea nitrate, guanidine nitrate, ethylenediamine dinitrate and ethanolamine dinitrate are used in explosives; and guanyl azide nitrate, 5-aminotetrazole nitrate, aminoguanidine nitrate, diaminoguanidine nitrate, dinitrate diguanidino-*s*-tetrazine and dinitrate-3,6-bis[(1*H*-1,2,3,4-tetrazol-5-yl)amino]-*s*-tetrazine are used in propellants and as gas generating agents (Tian *et al.*, 2011). Organic amine nitrates and organic amines differ in their physical and chemical properties, such as solubility, melting point, crystal structure, refractive index and reactivity. Bis(5-amino-1,2,4-triazol-3-yl)methane (BATZM) is an organic amine that falls into the class of energetic materials with a high decomposition temperature and detonation performance (Li *et al.*, 2020*b*). It can be used as a precursor for the synthesis of bis-triazole-based energetic materials (Dippold *et al.*, 2011; Zhao *et al.*, 2019). We wanted to explore what changes would occur when BATZM is reacted with nitric acid to form bis(5-amino-1,2,4-triazol-4-ium-3-yl)methane dinitrate, BATZM·$(NO_3)_2$. The crystal structure of BATZM·$(NO_3)_2$ was determined and the

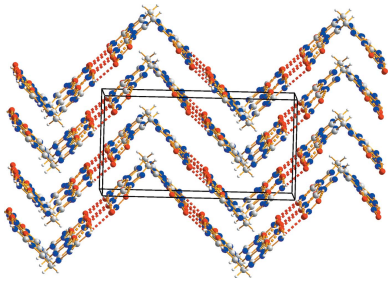

Table 1
Experimental details.

Crystal data	
Chemical formula	$C_5H_{10}N_8^{2+}\cdot 2NO_3^-$
M_r	306.23
Crystal system, space group	Orthorhombic, *Pbcn*
Temperature (K)	296
a, *b*, *c* (Å)	7.7416 (16), 8.9487 (18), 17.168 (3)
V (Å^3)	1189.3 (4)
Z	4
D_x (Mg m^{-3})	1.710
Radiation type	Mo *Kα*
μ (mm^{-1})	0.15
Crystal size (mm)	0.37 × 0.32 × 0.27
Data collection	
Diffractometer	Bruker APEXII CCD
Absorption correction	Multi-scan (*SADABS*; Bruker, 2009)
T_{min}, T_{max}	0.945, 0.959
No. of measured, independent and observed [$I > 2\sigma(I)$] reflections	6447, 1476, 1240
R_{int}	0.025
(sin $\theta/\lambda)_{max}$ (Å^{-1})	0.679
Refinement	
$R[F^2 > 2\sigma(F^2)]$, $wR(F^2)$, *S*	0.036, 0.103, 1.04
No. of reflections	1476
No. of parameters	117
H-atom treatment	All H-atom parameters refined
$\Delta\rho_{max}$, $\Delta\rho_{min}$ (e Å^{-3})	0.24, −0.17

Computer programs: *APEX2* (Bruker, 2009), *SAINT* (Bruker, 2009), *SHELXS97* (Sheldrick, 2008), *SHELXL2018* (Sheldrick, 2015) and *SHELXTL* (Sheldrick, 2008).

specific molar heat capacity ($C_{p,m}$) measured using the continuous C_p mode of a microcalorimeter and theoretical calculations. The detonation velocity (*D*) and pressure (*P*) of BATZM·$(NO_3)_2$ were also calculated to estimate its detonation properties. The above results are compared with those of BATZM and bis(5-amino-1,2,4-triazol-4-ium-3-yl)methane dichloride (BATZM·Cl_2), and the effect of nitrate formation on them is discussed.

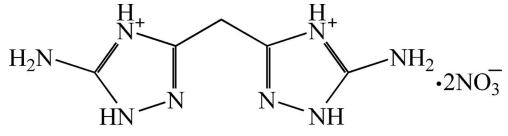

BATZM·$(NO_3)_2$

2. Experimental

Caution! Although BATZM and BATZM·$(NO_3)_2$ are rather stable against external stimuli, proper safety precautions should be taken when handling the dry materials. They are both energetic materials and tend to explode under the influence of heat, impact or friction. Laboratory personnel and equipment should be properly grounded, and protective equipment, such as earthed shoes, leather coats, gloves, ear protection and face shields, is recommended.

2.1. Materials

BATZM was synthesized and purified according to the method of Li *et al.* (2020*b*). Other chemicals and reagents used in the synthesis of BATZM·$(NO_3)_2$ were analytically pure and were used without further purification.

2.2. Synthesis and crystallization

For the preparation of BATZM·$(NO_3)_2$ used in this work, 68% HNO_3 (0.6 ml, 10.6 mmol) was added dropwise at room temperature to BATZM (0.721 g, 4 mmol) in deionized water (20 ml). The resulting solution was stirred for 2 h. Colourless rod-like crystals of BATZM·$(NO_3)_2$ were obtained by slow evaporation from water.

2.3. Characterization

Elemental analyses (C, H and N) were performed on an Elemental Analytical Instrument (PE-2400, PerkinElmer, USA). Analysis calculated (%) for $C_5H_{10}N_{10}O_6$: C 21.58, H 3.62, N 40.27; found: C 21.23, H 3.49, N 40.01. The oxygen balance of BATZM·$(NO_3)_2$ is −47%, which is higher than that of trinitrotoluene (TNT, −74%). Impact and friction-sensitivity measurements were obtained by employing a standard BAM Fallhammer and a BAM friction tester. The impact and friction sensitivity of BATZM·$(NO_3)_2$ are 10 J and 200 N, respectively, which are lower than for TNT (15 J and 353 N; Zhang *et al.*, 2017), indicating that its sensitivity is worse than TNT.

2.4. Refinement

Crystal data, data collection and structure refinement details are summarized in Table 1. All H atoms were originally found in difference maps.

2.5. Thermal decomposition conditions

The differential scanning calorimetry (DSC) and thermogravimetry/derivative thermogravimetry (TG/DTG) experiments on BATZM·$(NO_3)_2$ were determined using a Q600SDT (TA, USA) instrument at a pressure of 101.3 kPa under a nitrogen atmosphere and at a flow rate of 100 ml min^{-1}. The sample mass was 0.509 mg and the heating rate was 10.0 K min^{-1}. The temperature and heat were calibrated using

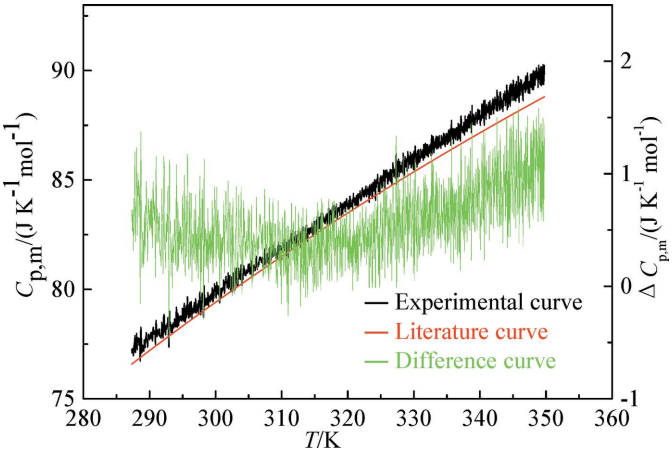

Figure 1
Experimental/literature/difference curves of the $C_{p,m}$ of α-Al_2O_3.

pure indium and tin particles. The DSC and TG/DTG curves obtained under the same conditions overlap well with each other and suggest that the reproducibility of the measurements is good.

2.6. Heat capacity determination

The $C_{p,m}$ of BATZM·$(NO_3)_2$ was determined using a continuous C_p mode from 283.15 to 353.15 K at a heating rate of 0.15 K min^{-1} on a Micro-DSCIII (Setaram, France) instrument with a sample mass of 201.70 mg at a pressure of 101.3 kPa. The microcalorimeter was calibrated with α-Al_2O_3 (calcined) using the mathematical expression C_p/(J K^{-1} mol^{-1}) = 18.82369 + 2.033349 × 10^{-1} (T/K) from 283.15 to 353.15 K, with the recommended equation C_p/(J K^{-1} mol^{-1}) = −1.32506 × 10^{8} (T/K)$^{-3}$ + 4.54238 × 10^{6} (T/K)$^{-2}$ − 5.475599 × 10^{4} (T/K)$^{-1}$ + 2.574076 × 10^{2} − 1.715032 × 10^{-1} (T/K) + 1.2897189 × 10^{-4} (T/K)^{2} − 4.60768 × 10^{-8} (T/K)^{3} + 6.31755 × 10^{-12} (T/K)^{4} from 283.15 to 353.15 K (Ditmars *et al.*, 1982) (Fig. 1). The difference between the experimental and recommended values range from −0.50 to 1.59 J K^{-1} mol^{-1} for temperatures from 283.15 to 353.15 K, and the standard uncertainty was calculated to be ±0.63 J K^{-1} mol^{-1} with a relative standard uncertainty of ±0.75%.

2.7. Quantum chemical calculations

The single-crystal structural data of BATZM·$(NO_3)_2$ were used in the theoretical calculations. The density functional theory (DFT) calculations were performed with the program package *DMol*^{3} in *Materials Studio* (Version 8.0) of Accelrys Inc. on a personal computer (Delley, 1990, 2000). The generalized gradient approximation (GGA) with the RPBE functional (Hammer *et al.*, 1999) and double-numerical quality basis set with polarization functions (DNP) were used for all the atoms, the size of DNP being comparable to Gaussian 6-31G**. A thermal smearing of 2.0 × 10^{-3} Hartree (Ha, 1 Ha = 27.2114 eV) and a real-space cut-off of 0.40 nm were adopted. For the numerical integration, the fine quality mesh size of the program was used. A 3 × 3 × 3 k-point sampling was applied in the geometry optimization (Andzelm *et al.*, 2001; Auckenthaler *et al.*, 2011; Baker *et al.*, 1996; Delley, 1996). The convergences of energy, gradient and maximal displacement were assigned as 10^{-5} Ha, 2.0 × 10^{-1} Ha Å^{-1} and 5.0 × 10^{-3} Å, respectively. In addition, the frequency analysis (Andzelm *et al.*, 2001; Baker *et al.*, 1996; Delley, 1996) was performed to check if the stationary point was a potential minimum and to obtain the thermodynamic properties at different temperatures under atmospheric pressure.

3. Results and discussion

3.1. Crystal structure

BATZM·$(NO_3)_2$ crystallizes in the orthorhombic space group *Pbcn* with Z = 4 and BATZM crystallizes in the orthorhombic space group *Fdd*2 with Z = 8 (Li *et al.*, 2020*b*). The molecular volume difference, ΔV, between BATZM·$(NO_3)_2$ and BATZM is 97.25 Å^3/molecule, and this result is assumed to be related to nitrate formation. The structures and reported molecular volume differences of other amines are also reported to be different from their nitrates. For example, the symmetry of adeninium dinitrate ($P2_12_12_1$; Hardgrove *et al.*, 1983) is higher than that of adenine ($P2_1/c$; Mahapatra *et al.*, 2008) and the ΔV between adeninium dinitrate (244.312 Å^3; Hardgrove *et al.*, 1983) and adenine (150.196 Å^3; Mahapatra *et al.*, 2008) is 94.116 Å^3/molecule; and the symmetry of cytosine ($P2_12_12_1$; McClure & Craven, 1973) is higher than that of cytosinium nitrate ($P\overline{1}$; Cherouana *et al.*, 2003) and the ΔV between cytosinium nitrate (179.721 Å^3; Cherouana *et al.*, 2003) and cytosine (118.106 Å^3; McClure & Craven, 1973) is 61.615 Å^3/molecule. The V of the nitric acid molecule is 55.166∼56.220 Å^3 (Allan *et al.*, 2010) at low temperature. Thus, the nitrate improves the space utilization to a more compressed structure.

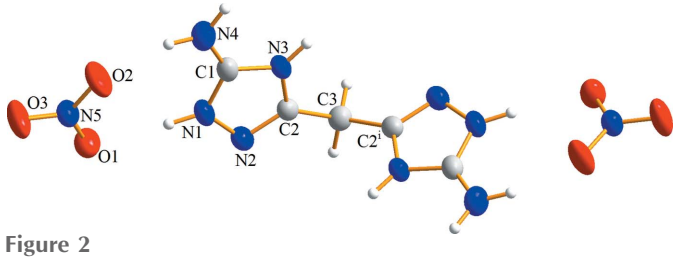

Figure 2
The molecular structure of BATZM·$(NO_3)_2$, with displacement ellipsoids drawn at the 50% probability level. [Symmetry code: (i) $-x$, y, $-z+\frac{1}{2}$.]

The molecules are characterized by two structural motifs: (i) internal symmetry and (ii) tight packing and extensive hydrogen bonding (Table 2); BATZM·$(NO_3)_2$, BATZM·Cl_2 and BATZM include these two structural motifs. Fig. 2 illustrates that the molecule of BATZM·$(NO_3)_2$ has an internal twofold axis which passes through atom C3 and is parallel to

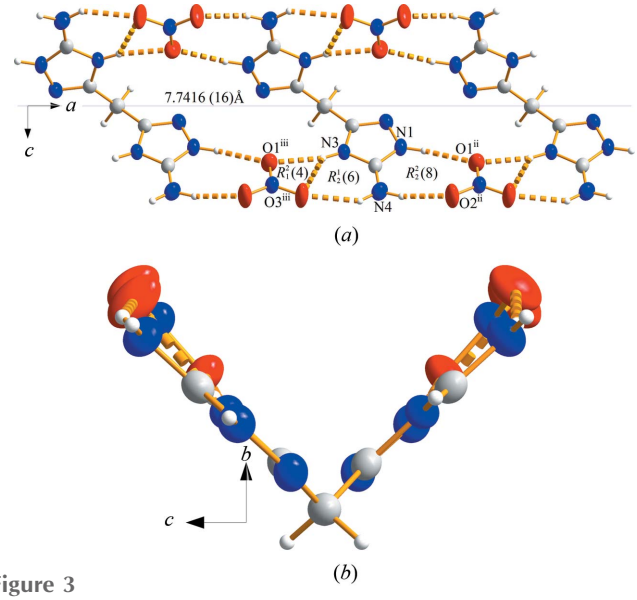

Figure 3
(*a*) The distance between adjacent molecules along the *a*-axis direction. (*b*) The 1D V-shaped chain of BATZM·$(NO_3)_2$. Displacement ellipsoids drawn at the 50% probability level. [Symmetry codes: (ii) x, $y+1$, z; (iii) $x-1$, $y+1$, z.]

Table 2
Hydrogen-bond geometry (Å, °).

D—H···A	D—H	H···A	D···A	D—H···A
N1—H1···O1^{ii}	0.897 (18)	2.138 (18)	3.0129 (15)	164.6 (14)
N4—H4A···O2^{ii}	0.874 (18)	1.986 (18)	2.8430 (17)	166.3 (15)
N3—H3···O1^{iii}	0.866 (17)	2.044 (17)	2.8962 (15)	167.6 (14)
N3—H3···O3^{iii}	0.866 (17)	2.325 (16)	2.9819 (16)	132.7 (13)
N4—H4B···O3^{iii}	0.89 (2)	2.20 (2)	2.9777 (18)	146.2 (17)
N4—H4B···O2^{iv}	0.89 (2)	2.32 (2)	3.0068 (18)	134.3 (17)

Symmetry codes: (ii) $x, y+1, z$; (iii) $x-1, y+1, z$; (iv) $x-\frac{1}{2}, -y+\frac{3}{2}, -z+1$.

the b axis, with reasonable chemical geometry and no disorder. The combination of H atoms with N3, which is the same as BATZM·Cl_2, also indicates that N3 has the highest charge density among all N atoms in the free base BATZM.

The BATZM$^+$ and NO_3^- ions, through five hydrogen bonds (N1—H1···O1^{ii}, N4—H4A···O2^{ii}, N3—H3···O1^{iii}, N3—H3···O3^{iii} and N4—H4B···O3^{iii}) and electrostatic attractions, form a one-dimensional (1D) V-shaped chain (Fig. 3*b*). The adjacent BATZM$^+$ ions have a translation along the a-axis direction (Fig. 3*a*). The 1D chain has three types of hydrogen bonds, including $R_2^2(8)$, $R_1^2(6)$ and $R_2^1(4)$ hydrogen-bond graph-set motifs, according to the definition of Bernstein *et al.* (1995). The N4—H4B···O2^{iv} hydrogen bond connects adjacent 1D V-shaped chains (Fig. 4*a*) to form a two-dimensional (2D) corrugated sheet (Fig. 4*b*). Two adjacent 1D V-shaped chains have a 2_1 screw axis along the a-axis direction and two alternate 1D V-shaped chains have a translation along the c-axis direction (Fig. 4*b*).

The packing diagram of BATZM·$(NO_3)_2$, viewed down the a axis, is shown in Fig. 5 and illustrates that the 2D corrugated sheet formed through van der Waals forces forms a three-dimensional (3D) network. The distance between adjacent 2D corrugated sheets is half of the b unit-cell length and two alternate 2D corrugated sheets have a translation along the b-axis direction. The angle between the two triazole ring planes is 85.11 (3)°, with an internal C2—C3—C2^i angle of 115.80 (14)° and the intramolecular contact distance C1···C1^i is 5.8424 (16) Å [symmetry code: (i) $-x, y, -z+\frac{1}{2}$]. The corresponding values for BATZM are 77.21 (4)°, 111.2 (2)° and 5.635 (2) Å, respectively (Li *et al.*, 2020*b*). The electrostatic repulsion of NO_3^- and NO_3^-, and of amine cations and amine cations of adjacent 2D corrugated sheets lead to repulsion of the triazole rings, so the angle between the two triazole ring planes, the C1···C1^i distance and the C2—C3—C2^i angle all become larger.

3.2. Thermal behaviour

The DSC and TG/DTG curves for BATZM·$(NO_3)_2$ at a heating rate of 10.0 K min^{-1} are not unusual (Figs. 6 and 7). The DSC curve indicates that the thermal behaviour can be divided into three consecutive exothermic decomposition stages. The extrapolated onset temperature (T_e) and peak temperature (T_p) of the first exothermic decomposition stage are determined as 499.68 and 508.4 K, respectively. The decomposition temperature of BATZM is 566.15 K (Shreve & Charlesworth, 1956). Compared to the free base, the thermal stability is reduced after nitrate formation and is just a little higher than for BATZM·Cl_2 (493.15 K) (Li *et al.*, 2020*a*). The decomposition temperature of TNT is 568.15 K (Wang *et al.*, 2010), indicating that the thermal stability of BATZM·$(NO_3)_2$ is worse than that of TNT. The T_e and T_p values of the second stage are 514.80 and 519.06 K, respectively, and of the last stage are 557.01 and 603.55 K, respectively. The TG plot shows that the three stages have a mass loss of 54.67%.

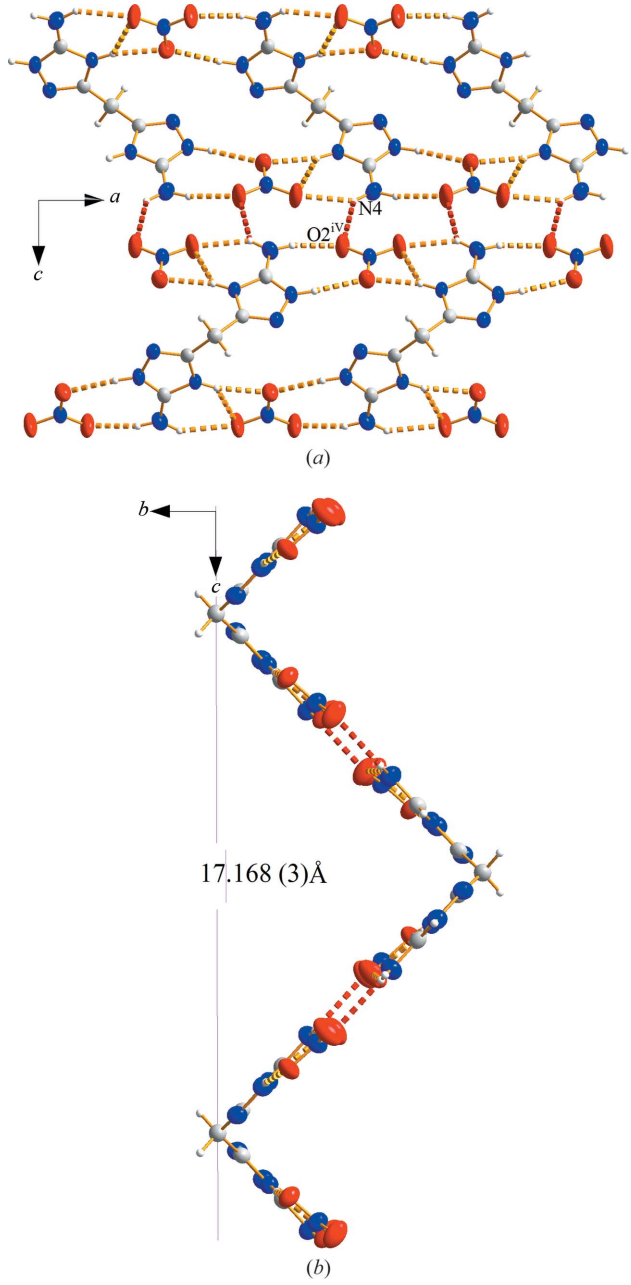

Figure 4
(*a*) The hydrogen bond connecting adjacent 1D V-shaped chains. (*b*) The 2D corrugated sheet of BATZM·$(NO_3)_2$. The distance highlighted is that between alternate molecules along the c-axis direction. Displacement ellipsoids drawn at the 50% probability level. [Symmetry code: (iv) $x-\frac{1}{2}, -y+\frac{3}{2}, -z+1$.]

Table 3
Thermodynamic properties of BATZM·$(NO_3)_2$ at a pressure of 101.3 kPa.

T (K)	$C_{p,m}$ (J K^{-1} mol^{-1})		RD	$H_T - H_{298.15K}$ (kJ mol^{-1})		RD	$S_T - S_{298.15K}$ (J K^{-1} mol^{-1})		RD
	Exp	Calc		Exp	Calc		Exp	Calc	
288.15	354.99	310.74	12.47	−3.61	−3.15	12.76	−12.31	−10.74	12.72
293.15	360.87	314.80	12.77	−1.82	−1.58	12.87	−6.15	−5.36	12.83
298.15	366.14	318.84	12.92	–	–	–	–	–	–
303.15	370.93	322.86	12.96	1.84	1.60	12.97	6.13	5.34	12.92
308.15	375.34	326.85	12.92	3.71	3.23	12.97	12.23	10.65	12.93
313.15	379.49	330.82	12.83	5.60	4.87	12.94	18.31	15.95	12.91
318.15	383.50	334.76	12.71	7.50	6.54	12.90	24.35	21.22	12.87
323.15	387.46	338.68	12.59	9.43	8.22	12.84	30.36	26.47	12.83
328.15	391.51	342.58	12.50	11.38	9.92	12.78	36.34	31.69	12.79
333.15	395.75	346.45	12.46	13.35	11.65	12.72	42.30	36.90	12.76
338.15	400.29	350.30	12.49	15.34	13.39	12.67	48.22	42.08	12.74
343.15	405.26	354.12	12.62	17.35	15.16	12.64	54.14	47.24	12.73
348.15	410.75	357.93	12.86	19.39	16.94	12.62	60.04	52.38	12.75

Notes: 'Exp' is the result of an experimental determination; 'Calc' is the result of a theoretical calculation; RD = $10^2(X_{Exp} - X_{Calc})/X_{Exp}$; $H_T - H_{298.15K}$ is the enthalpy change when taking 298.15 K as the benchmark; $S_T - S_{298.15K}$ is the entropy change when taking 298.15 K as the benchmark.

3.3. Specific heat capacity

The $C_{p,m}$ of BATZM·$(NO_3)_2$ was measured using the continuous C_p mode of a Micro-DSCIII apparatus and is shown in Fig. 8. It was found that the $C_{p,m}$ of BATZM·$(NO_3)_2$ is satisfactorily modelled by a cubic relationship between the temperatures 287.60 and 349.73 K, and the $C_{p,m}$ equation can be defined as:

$$C_{p,m}[\text{BATZM}\cdot(NO_3)_2]/(\text{J K}^{-1}\ \text{mol}^{-1}) = -4.80978\times10^3 + 4.71622\times10\,(T/\text{K}) - 1.45050\times10^{-1}\,(T/\text{K})^2 + 1.51244\times10^{-4}\,(T/\text{K})^3 \quad (1)$$

The correlation coefficients of the fitting (R^2) and the standard deviation (SD) results are 0.99804 and 0.70492, respectively. The $C_{p,m}$ value of a compound can be influenced by many factors, such as formula weight, component elements, molecular structure and substituent position. The $\Delta C_{p,m}$ between an amine and its nitrate is not constant. For example, at 298.15 K, the $\Delta C_{p,m}$ (all values in J K^{-1} mol^{-1}) between diglycine nitrate (297.0; Taraskin *et al.*, 1985) and glycine (198.6; Spink & Wadsö, 1975) is 98.4, between acetamidium nitrate (175.0; Nurachmetov *et al.*, 1985) and acetamide (91.27; Nurachmetov *et al.*, 1985) is 83.73, between thiouronium nitrate (175.4; Nurachmetov *et al.*, 1984) and thiourea (96.9; Gomez & Sabbah, 1982) is 78.5, and between uronium nitrate (158.6; Nurachmetov *et al.*, 1985) and urea (92.76; Andersson *et al.*, 1993) is 65.81. At 298.15 K, the $\Delta C_{p,m}$ between BATZM·$(NO_3)_2$ (366.14) and BATZM (211.19; Li *et al.*, 2020*b*) is 154.95, and presumably the difference is larger due to the nitrate ion and H-atom interactions, as well as changes in the molecular structure.

Table 3 shows a comparison between the $C_{p,m}$ value of BATZM·$(NO_3)_2$ obtained by theoretical calculation (labelled 'Calc') and experimental determination (labelled 'Exp'), and their relative differences (RD) at different temperatures. The theoretical calculation results are all less than the experimentally determined results, and the relative deviations vary from 12.46 to 12.96%. These results are similar to those observed for *N*-benzoyl-3,3-dinitroazetidine (Yan *et al.*, 2012),

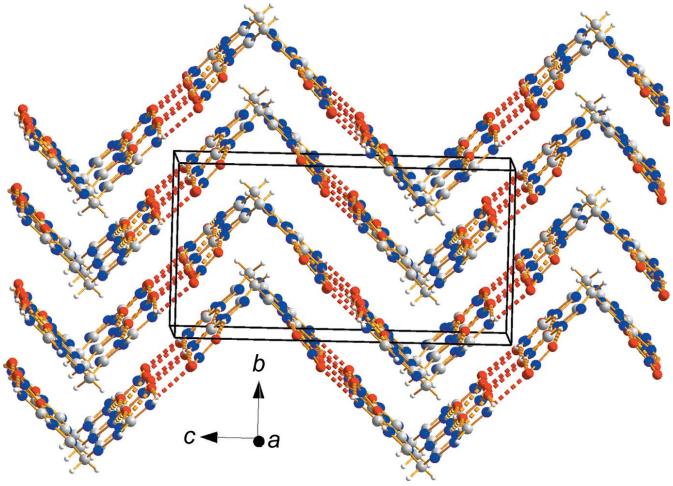

Figure 5
Packing diagram of BATZM·$(NO_3)_2$.

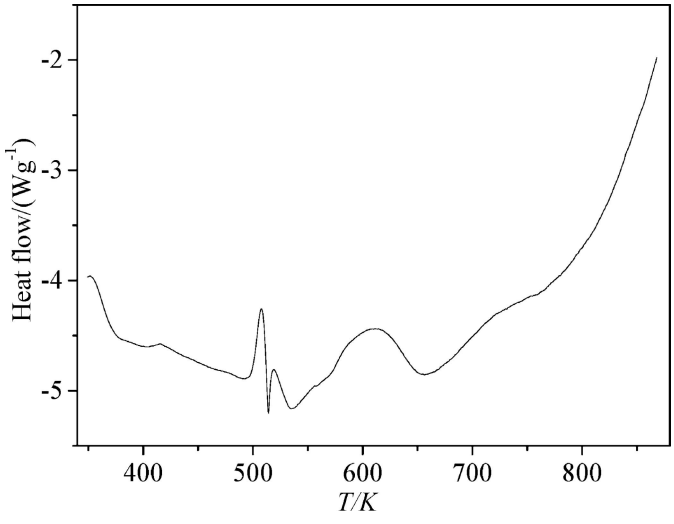

Figure 6
DSC curve of BATZM·$(NO_3)_2$ at a heating rate of 10.0 K min^{-1}.

Table 4
Nitrogen equivalents of different detonation products.

Detonation product	C	H_2O	N_2	CO	CO_2
Nitrogen equivalent index	0.15	0.54	1	0.78	1.35

N-(2,4-dinitrophenyl)-3,3-dinitroazetidine (Yan *et al.*, 2014), *N*-acetyl-3,3-dinitroazetidine (Li *et al.*, 2015), hexaconazole (Yan *et al.*, 2016*a*), myclobutanil (Yan *et al.*, 2016*a*), diniconazole (Yan *et al.*, 2016*b*), 3,3-dinitroazetidinium perchlorate (Yan *et al.*, 2016*c*), 3,3-dinitroazetidinium chloride (Yan *et al.*, 2016*c*), BATZM (Li *et al.*, 2020*b*) and BATZM·Cl_2 (Li *et al.*, 2020*a*).

3.4. Thermodynamic properties

The enthalpy change and entropy change of BATZM·-$(NO_3)_2$ were calculated using Equations (2) and (3) from 288.15 to 348.15 K and taking 298.15 K as the benchmark; the results are listed in Table 3. The absolute values of the theoretical calculations of BATZM·$(NO_3)_2$ are all lower than those of the experimental determination, and the relative deviations of $H_T - H_{298.15K}$ and $S_T - S_{298.15K}$ of BATZM·$(NO_3)_2$ are almost equivalent at each temperature, and their relative deviations (12.62–12.97%) vary only slightly.

$$H_T - H_{2.98.15K}/\left(\mathrm{J\ mol^{-1}}\right) = \int_{298.15K}^{T} C_{p,\mathrm{m}}\mathrm{d}T/\left(\mathrm{J\ mol^{-1}}\right) \quad (2)$$

$$S_T - S_{298.15K}/\left(\mathrm{J\ K^{-1}\ mol^{-1}}\right) = \int_{298.15K}^{T} C_{p,\mathrm{m}} \cdot T^{-1}\mathrm{d}T/\left(\mathrm{J\ K^{-1}\ mol^{-1}}\right) \quad (3)$$

3.5. Characterization of detonation velocity and pressure

Detonation velocity (D) and pressure (P) are the most important parameters for describing the detonation characteristics of energetic materials. The D and P values of an explosive can be predicted by the nitrogen equivalent equation shown as Equations (4) to (6) (Guo & Zhang, 1983).

$$\Sigma N = 100\Sigma x_i N_i/M \quad (4)$$

$$D = (690 + 1160\rho)\Sigma N \quad (5)$$

$$P = 1.092(\rho\Sigma N)^2 - 0.574 \quad (6)$$

where $\sum N$ is the nitrogen equivalent of the detonation products, x_i is the mole number of a certain detonation product produced by a mole explosive, N_i is the nitrogen equivalent index of a certain detonation product, M is the molecular weight of an explosive (g mol^{-1}) and ρ is the density of an explosive (g cm^{-3}).

The detonation products produced by explosives, together with their nitrogen equivalent indices, are listed in Table 4. According to the order $H_2O \rightarrow CO \rightarrow CO_2$ in forming detonation products, the detonation products of BATZM·$(NO_3)_2$ are calculated as follows:

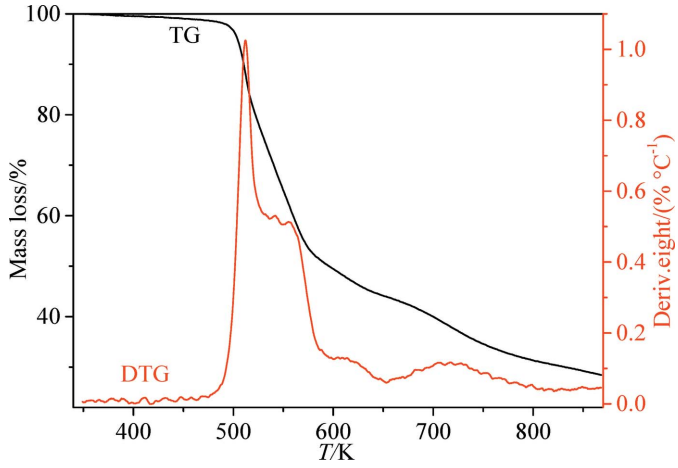

Figure 7
TG/DTG curves of BATZM·$(NO_3)_2$ at a heating rate of 10.0 K min^{-1}.

$$C_5H_{10}N_{10}O_6 = (4)C + (1)CO + (5)H_2O + (5)N_2.$$

According to Equation (4), in which M = 306.23 g mol^{-1} and $\rho = 1.710 \pm 0.001$ g cm^{-3} (the density is obtained from X-ray data), the total nitrogen equivalents of BATZM·$(NO_3)_2$ are obtained through the nitrogen equivalent indices of the detonation products in Table 4:

$$\sum N = 100 \times (4 \times 0.15 + 1 \times 0.78 + 5 \times 0.54 + 5 \times 1)/\ 306.23 = 2.965.$$

The D and P values can be obtained according to Equations (5) and (6), *viz.* 7927.47 ± 3.63 m s^{-1} and 27.50 ± 0.03 GPa, respectively, which are greater than these of TNT (6881 m s^{-1} and 19.5 GPa; Wang *et al.*, 2010), BATZM (7954.87 ± 3.29 m s^{-1} and 25.72 ± 0.03 GPa; Li *et al.*, 2020*b*) and BATZM·Cl_2 (7143.60 ± 3.66 m s^{-1} and 21.49 ± 0.03 GPa; Li

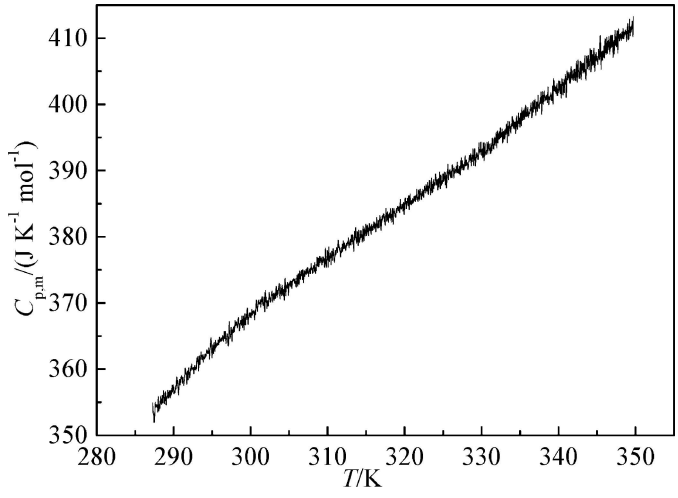

Figure 8
Determination of the continuous $C_{p,\mathrm{m}}$ of BATZM·$(NO_3)_2$.

et al., 2020*a*) and less than those of 1,3,5-triamino-2,4,6-trinitrobenzene (TATB; 8114 m s^{-1} and 31.2 GPa; Wang *et al.*, 2010). This indicates that the explosive energy of the compound is increased after nitrate formation.

4. Conclusions

The structure of BATZM·$(NO_3)_2$ is found to crystallize in the space group *Pbcn* (orthorhombic) with a highly dense 1D V-shaped chain and a 2D corrugated sheet. Its decomposition temperature is 498.01 K. Its $C_{p,m}$ equation is $C_{p,m}/(J\,K^{-1}\,mol^{-1}) = -4.80978 \times 10^3 + 4.71622 \times 10\,(T/K) - 1.45050 \times 10^{-1}\,(T/K)^2 + 1.51244 \times 10^{-4}\,(T/K)^3$ and the $C_{p,m}$ value is 366.14 J K^{-1} mol^{-1} at 298.15 K. The relative deviations of the $C_{p,m}$, $H_T - H_{298.15K}$ and $S_T - S_{298.15K}$ of BATZM·$(NO_3)_2$ are almost equivalent at each temperature and their relative deviations change little. The D and P values are found to be 7927.47 ± 3.63 m s^{-1} and 27.50 ± 0.03 GPa, respectively. The above results of BATZM·$(NO_3)_2$ were compared with those of BATZM and indicate that the specific heat capacity becomes larger, the thermal stability becomes worse and the energy increases after nitrate formation. The performance of BATZM·$(NO_3)_2$ is better than BATZM·Cl_2 as an energetic material. Based on the detonation properties, it has a better performance than TNT, but the sensitivity and thermal stability of TNT are better than those of BATZM·$(NO_3)_2$.

Funding information

Funding for this research was provided by: National Natural Science Foundation of China (grant Nos. 21673179, 21663033 and 51762042); Provincial Natural Science Foundation of Shaanxi (grant Nos. 2019SF-271 and 2018JZ2004); Key Laboratory Project Foundation of Shaanxi Provincial Education Department in China (grant No. 20JS158); Startup Foundation for Advanced Talents of Yulin University (grant No. 16GK10).

References

Allan, D. R., Marshall, W. G., Francis, D. J., Oswald, I. D. H., Pulham, C. R. & Spanswick, C. (2010). *Dalton Trans.* **39**, 3736–3743.
Andersson, O., Matsuo, T., Suga, H. & Ferloni, P. (1993). *Int. J. Thermophys.* **14**, 149–158.
Andzelm, J., King-Smith, R. D. & Fitzgerald, G. (2001). *Chem. Phys. Lett.* **335**, 321–326.
Auckenthaler, T., Blum, V., Bungartz, H. J., Huckle, T., Johanni, R., Krämer, L., Lang, B., Lederer, H. & Willems, P. R. (2011). *Parallel Comput.* **37**, 783–794.
Baker, J., Kessi, A. & Delley, B. (1996). *J. Chem. Phys.* **105**, 192–212.
Bernstein, J., Davis, R. E., Shimoni, L. & Chang, N.-L. (1995). *Angew. Chem. Int. Ed. Engl.* **34**, 1555–1573.
Bruker (2009). *APEX2*, *SAINT* and *SADABS*. Bruker AXS Inc., Madison, Wisconsin, USA.
Cherouana, A., Bouchouit, K., Bendjeddou, L. & Benali-Cherif, N. (2003). *Acta Cryst.* E**59**, o983–o985.
Delley, B. (1990). *J. Chem. Phys.* **92**, 508–517.
Delley, B. (1996). *J. Phys. Chem.* **100**, 6107–6110.
Delley, B. (2000). *J. Chem. Phys.* **113**, 7756–7764.
Dippold, A. A., Feller, M. & Klapötke, T. M. (2011). *Cent. Eur. J. Energ. Mat.* **8**, 261–278.
Ditmars, D. A., Ishihara, S., Chang, S.-S., Bernstein, G. & West, E. D. (1982). *J. Res. Natl Bur. Stand.* **87**, 159–163.
Gomez, L. A. T. & Sabbah, R. (1982). *Thermochim. Acta*, **57**, 67–81.
Guo, Y.-X. & Zhang, H.-S. (1983). *Explos. Shock Waves*, **3**, 5623–5629.
Hammer, B., Hansen, L. B. & Nørskov, J. K. (1999). *Phys. Rev. B*, **59**, 7413–7421.
Hardgrove, G. L., Einstein, J. R., Hingerty, B. E. & Wei, C. H. (1983). *Acta Cryst.* C**39**, 88–90.
Li, H., Yan, B., Ma, H., Ma, X., Sun, Z. & Ma, Y. (2020*a*). *Acta Cryst.* C**76**, 821–827.
Li, H., Yan, B., Ma, H., Sun, Z., Ma, Y. & Zhang, Z. (2020*b*). *Acta Cryst.* C**76**, 64–68.
Li, H.-Y., Yan, B., Bai, K.-Q., Liu, H., Ma, H.-X., Song, J.-R. & Yan, L. (2015). *J. Chem. Thermodyn.* **91**, 240–244.
Mahapatra, S., Nayak, S. K., Prathapa, S. J. & Guru Row, T. N. (2008). *Cryst. Growth Des.* **8**, 1223–1225.
McClure, R. J. & Craven, B. M. (1973). *Acta Cryst.* B**29**, 1234–1238.
Nurachmetov, N. N., Beremzhanov, B. A., Abramova, G. V. & Lebedev, B. V. (1984). *Probl. Kalorim. Khim. Termodin. Dokl. Vses. Konf.* 10th, **2**, 460–462.
Nurachmetov, N. N., Beremzhanov, B. A., Abramova, G. V. & Lebedev, B. V. (1985). *Thermochim. Acta*, **92**, 329–332.
Sheldrick, G. M. (2008). *Acta Cryst.* A**64**, 112–122.
Sheldrick, G. M. (2015). *Acta Cryst.* C**71**, 3–8.
Shreve, R. N. & Charlesworth, R. K. (1956). US Patent 2744116.
Spink, C. H. & Wadsö, I. (1975). *J. Chem. Thermodyn.* **7**, 561–572.
Taraskin, S. A., Savilova, Z. V., Strukov, B. A. & Varikash, V. M. (1985). *Izv. Akad. Nauk SSSR Ser. Fiz.* **49**, 268–271.
Tian, D. Y., Zhao, F. Q. & Liu, J. H. (2011). In *Handbook of Energetic Materials and the Related Compounds*. Beijing: National Defense Industry Press.
Wang, R.-H., Xu, H.-Y., Guo, Y., Sa, R.-J. & Shreeve, J. M. (2010). *J. Am. Chem. Soc.* **132**, 11904–11905.
Yan, B., Li, H.-Y., Gao, J., Wang, A.-M., Ren, G.-Y., Li, Y.-J. & Ma, H.-X. (2016*a*). *J. Chem. Thermodyn.* **99**, 82–85.
Yan, B., Li, H.-Y., Guan, Y.-L., Ma, H.-X., Song, J.-R. & Zhao, F.-Q. (2016*b*). *J. Chem. Thermodyn.* **103**, 206–211.
Yan, B., Li, H.-Y., Zhao, N.-N., Ma, H.-X., Song, J.-R., Zhao, F.-Q. & Hu, R.-Z. (2014). *J. Chem. Thermodyn.* **69**, 152–156.
Yan, B., Li, J., Li, H.-Y., Gao, J., Wang, A.-M., Ren, G.-Y. & Ma, H.-X. (2016*c*). *J. Chem. Thermodyn.* **101**, 44–48.
Yan, B., Zhao, N.-N., Mai, T., Xu, K.-Z., Ma, H.-X. & Song, J.-R. (2012). *Russ. J. Phys. Chem. A*, **86**, 1962–1968.
Zhang, Y.-L., Zhang, S., Sun, L., Yang, Q., Han, J., Wei, Q., Xie, G., Chen, S.-P. & Gao, S.-L. (2017). *Chem. Commun.* **53**, 3034–3037.
Zhao, G., Yin, P., Kumar, D., Imler, G. H., Parrish, D. A. & Shreeve, J. M. (2019). *J. Am. Chem. Soc.* **141**, 19581–19584.

supporting information

Acta Cryst. (2020). C**76**, 965-971 [https://doi.org/10.1107/S2053229620012516]

Crystal structure, thermal properties and detonation characterization of bis(5-amino-1,2,4-triazol-4-ium-3-yl)methane dinitrate

Hongya Li, Biao Yan, Haixia Ma, Xiangrong Ma, Zhiyong Sun and Yajun Ma

Computing details

Data collection: *APEX2* (Bruker, 2009); cell refinement: *SAINT* (Bruker, 2009); data reduction: *SAINT* (Bruker, 2009); program(s) used to solve structure: *SHELXS97* (Sheldrick, 2008); program(s) used to refine structure: *SHELXL2018* (Sheldrick, 2015); molecular graphics: *SHELXTL* (Sheldrick, 2008); software used to prepare material for publication: *SHELXTL* (Sheldrick, 2008).

Methylenebis(5-amino-1,2,4-triazol-4-ium) dinitrate

Crystal data

$C_5H_{10}N_8^{2+}\cdot 2NO_3^-$
M_r = 306.23
Orthorhombic, *Pbcn*
a = 7.7416 (16) Å
b = 8.9487 (18) Å
c = 17.168 (3) Å
V = 1189.3 (4) Å^3
Z = 4
F(000) = 632
D_x = 1.710 Mg m^{-3}
Mo *Kα* radiation, λ = 0.71073 Å
Cell parameters from 2960 reflections
θ = 2.6–28.7°
μ = 0.15 mm^{-1}
T = 296 K
Rodlike, colourless
0.37 × 0.32 × 0.27 mm

Data collection

Bruker APEXII CCD diffractometer
φ and ω scans
Absorption correction: multi-scan (SADABS; Bruker, 2009)
T_{min} = 0.945, T_{max} = 0.959
6447 measured reflections
1476 independent reflections
1240 reflections with $I > 2\sigma(I)$
R_{int} = 0.025
θ_{max} = 28.9°, θ_{min} = 3.5°
h = −9→9
k = −11→12
l = −11→23

Refinement

Refinement on F^2
Least-squares matrix: full
$R[F^2 > 2\sigma(F^2)]$ = 0.036
$wR(F^2)$ = 0.103
S = 1.03
1476 reflections
117 parameters
0 restraints
Primary atom site location: structure-invariant direct methods
Secondary atom site location: difference Fourier map
Hydrogen site location: difference Fourier map
All H-atom parameters refined
$w = 1/[\sigma^2(F_o^2) + (0.0527P)^2 + 0.2645P]$ where $P = (F_o^2 + 2F_c^2)/3$
$(\Delta/\sigma)_{max} < 0.001$
$\Delta\rho_{max}$ = 0.24 e Å^{-3}
$\Delta\rho_{min}$ = −0.17 e Å^{-3}
Extinction correction: SHELXL2018 (Sheldrick, 2015), $Fc^*=kFc[1+0.001xFc^2\lambda^3/\sin(2\theta)]^{-1/4}$
Extinction coefficient: 0.0093 (17)

Special details

Geometry. All esds (except the esd in the dihedral angle between two l.s. planes) are estimated using the full covariance matrix. The cell esds are taken into account individually in the estimation of esds in distances, angles and torsion angles; correlations between esds in cell parameters are only used when they are defined by crystal symmetry. An approximate (isotropic) treatment of cell esds is used for estimating esds involving l.s. planes.

Fractional atomic coordinates and isotropic or equivalent isotropic displacement parameters (Å²)

	x	*y*	*z*	U_{iso}*/U_{eq}
N4	0.26604 (17)	1.09743 (15)	0.43580 (8)	0.0483 (3)
N3	0.09405 (13)	0.94979 (11)	0.34993 (6)	0.0336 (3)
N2	0.29749 (14)	0.83162 (13)	0.28447 (6)	0.0399 (3)
N1	0.36750 (14)	0.92772 (13)	0.33965 (6)	0.0403 (3)
N5	0.74687 (13)	0.12768 (14)	0.42174 (6)	0.0408 (3)
O3	0.89030 (13)	0.16661 (16)	0.44456 (8)	0.0718 (4)
O1	0.73330 (12)	0.02284 (12)	0.37331 (6)	0.0483 (3)
O2	0.61582 (13)	0.19240 (14)	0.44553 (7)	0.0629 (4)
C1	0.24492 (15)	0.99885 (14)	0.37944 (7)	0.0340 (3)
C2	0.13286 (15)	0.84798 (12)	0.29291 (6)	0.0316 (3)
C3	0.000000	0.75929 (19)	0.250000	0.0362 (4)
H3A	0.064 (2)	0.6949 (16)	0.2119 (8)	0.046 (4)*
H1	0.481 (2)	0.9381 (17)	0.3474 (9)	0.055 (5)*
H3	−0.009 (2)	0.9775 (17)	0.3636 (8)	0.047 (4)*
H4A	0.373 (2)	1.1206 (18)	0.4467 (9)	0.053 (5)*
H4B	0.170 (3)	1.136 (2)	0.4566 (11)	0.073 (6)*

Atomic displacement parameters (Å²)

	U^{11}	U^{22}	U^{33}	U^{12}	U^{13}	U^{23}
N4	0.0406 (7)	0.0527 (7)	0.0515 (7)	−0.0065 (6)	−0.0070 (5)	−0.0093 (6)
N3	0.0237 (5)	0.0381 (5)	0.0389 (5)	0.0004 (4)	0.0012 (4)	−0.0021 (4)
N2	0.0304 (6)	0.0494 (6)	0.0400 (5)	0.0052 (5)	0.0019 (4)	0.0002 (4)
N1	0.0241 (5)	0.0505 (6)	0.0464 (6)	0.0001 (5)	−0.0017 (4)	0.0022 (5)
N5	0.0286 (6)	0.0491 (6)	0.0448 (6)	0.0042 (4)	−0.0017 (4)	−0.0078 (5)
O3	0.0269 (6)	0.0951 (9)	0.0935 (9)	0.0014 (5)	−0.0084 (5)	−0.0426 (7)
O1	0.0403 (6)	0.0526 (6)	0.0521 (6)	0.0050 (4)	−0.0031 (4)	−0.0163 (5)
O2	0.0295 (6)	0.0701 (7)	0.0890 (8)	0.0077 (5)	0.0034 (5)	−0.0324 (6)
C1	0.0289 (6)	0.0367 (6)	0.0363 (6)	−0.0020 (5)	−0.0019 (4)	0.0060 (5)
C2	0.0288 (6)	0.0351 (6)	0.0310 (5)	0.0036 (5)	−0.0001 (4)	0.0037 (4)
C3	0.0357 (9)	0.0359 (8)	0.0370 (8)	0.000	−0.0021 (6)	0.000

Geometric parameters (Å, º)

N4—C1	1.3195 (18)	N1—C1	1.3313 (17)
N4—H4A	0.874 (18)	N1—H1	0.897 (18)
N4—H4B	0.89 (2)	N5—O3	1.2279 (14)
N3—C1	1.3467 (15)	N5—O2	1.2375 (14)
N3—C2	1.3706 (15)	N5—O1	1.2580 (15)

N3—H3	0.866 (17)	C2—C3	1.4935 (14)
N2—C2	1.2911 (16)	C3—H3A	1.003 (14)
N2—N1	1.3896 (15)	C3—H3A^{i}	1.003 (14)
C1—N4—H4A	115.6 (11)	N4—C1—N1	127.42 (12)
C1—N4—H4B	116.7 (13)	N4—C1—N3	126.96 (12)
H4A—N4—H4B	127.6 (18)	N1—C1—N3	105.62 (11)
C1—N3—C2	107.17 (10)	N2—C2—N3	111.84 (10)
C1—N3—H3	127.0 (10)	N2—C2—C3	124.35 (10)
C2—N3—H3	125.8 (10)	N3—C2—C3	123.68 (10)
C2—N2—N1	103.79 (10)	C2^{i}—C3—C2	115.80 (14)
C1—N1—N2	111.57 (10)	C2^{i}—C3—H3A	108.9 (8)
C1—N1—H1	125.1 (10)	C2—C3—H3A	106.7 (8)
N2—N1—H1	123.3 (10)	C2^{i}—C3—H3A^{i}	106.7 (8)
O3—N5—O2	120.22 (12)	C2—C3—H3A^{i}	108.9 (8)
O3—N5—O1	119.86 (11)	H3A—C3—H3A^{i}	109.8 (16)
O2—N5—O1	119.91 (11)		
C2—N2—N1—C1	−0.06 (13)	N1—N2—C2—C3	−175.48 (10)
N2—N1—C1—N4	179.97 (12)	C1—N3—C2—N2	−0.66 (13)
N2—N1—C1—N3	−0.33 (14)	C1—N3—C2—C3	175.29 (10)
C2—N3—C1—N4	−179.72 (12)	N2—C2—C3—C2^{i}	−126.21 (12)
C2—N3—C1—N1	0.58 (13)	N3—C2—C3—C2^{i}	58.34 (9)
N1—N2—C2—N3	0.44 (13)		

Symmetry code: (i) −*x*, *y*, −*z*+1/2.

Hydrogen-bond geometry (Å, º)

D—H···*A*	*D*—H	H···*A*	*D*···*A*	*D*—H···*A*
N1—H1···O1^{ii}	0.897 (18)	2.138 (18)	3.0129 (15)	164.6 (14)
N4—H4*A*···O2^{ii}	0.874 (18)	1.986 (18)	2.8430 (17)	166.3 (15)
N3—H3···O1^{iii}	0.866 (17)	2.044 (17)	2.8962 (15)	167.6 (14)
N3—H3···O3^{iii}	0.866 (17)	2.325 (16)	2.9819 (16)	132.7 (13)
N4—H4*B*···O3^{iii}	0.89 (2)	2.20 (2)	2.9777 (18)	146.2 (17)
N4—H4*B*···O2^{iv}	0.89 (2)	2.32 (2)	3.0068 (18)	134.3 (17)

Symmetry codes: (ii) *x*, *y*+1, *z*; (iii) *x*−1, *y*+1, *z*; (iv) *x*−1/2, −*y*+3/2, −*z*+1.